Desalination and Water Treatment
www.deswater.com

doi: 10.5004/dwt.2022.28440

259 (2022) 17–36
May

Commercial antiscalants used for scaling mitigation of $CaCO_3$ during the membrane distillation treatment of reverse osmosis brine

Chang Liu[a,*], Shanfu Tang[a], Liang Zhu[b,c], Rongping Ji[a]

[a]*College of Environmental Science and Engineering, Yangzhou University, Yangzhou 225127, P.R. China, emails: liu_chang@yzu.edu.cn (C. Liu), 651991549@qq.com (S.F. Tang), 3228632223@qq.com (R.P. Ji)*
[b]*Key Laboratory of Integrated Regulation and Resources Development of Shallow Lakes, Hohai University, Nanjing 210098, China, email: hhuzhuliang@163.com (L. Zhu)*
[c]*College of Environment, Hohai University, Nanjing 210098, China*

Received 8 November 2021; Accepted 27 March 2022

ABSTRACT

Although membrane distillation technique (MD) exhibited significant potential for desalination of reverse osmosis (RO) brine, the occurrences of $CaCO_3$ scaling and subsequent membrane wetting have significantly restricted the practical application of MD. As antiscalants are widely applied for scaling control in RO devices, it is meaningful to study the anti-scaling performance of antiscalants during the MD process of RO brine. In this study, 1-hydroxyethylidene-1,1-diphosphonic acid (HEDP), polyamino polyether methylene phosphonic acid (PAPEMP), and hydrolyzed polymaleic anhydride (HPMA) were applied to investigate impacts of antiscalants addition on permeate flux, feed water quality, distillate conductivity, crystal structure, and scaling layer development in a MD plant. The influences of feed temperature and antiscalants dosage on the $CaCO_3$ mitigation performance of three antiscalants were studied in 40°C–90°C and 5–100 mg/L, respectively. The results revealed that these three antiscalants all efficiently alleviated flux drop and increment of permeation conductivity. HPMA and PAPEMP exceeded HEDP in mitigating $CaCO_3$ scaling by transforming crystal form from stable calcite to labile vaterite and aragonite. The antiscalant dosage exhibited remarkable impacts on $CaCO_3$ scaling inhibition and the anti-scaling performance was superb at a dosage of <20 mg/L for HEDP and HPMA. Comparatively, PAPEMP and HPMA posed greater tolerance to feed temperature than HEDP.

Keywords: Membrane distillation; Reverse osmosis brine; Calcium carbonate scaling; Antiscalants; Feed temperature

1. Introduction

Desalination of seawater or brackish water has been extensively implemented in many water-deficient regions for secure drinking water supply, and the reverse osmosis (RO) technology occupied more than 50% of existing desalination plants [1,2]. However, a mass of brine generated from RO process has caused several environmental issues, and sustainable brine management strategies are desiderated to minimize and treat RO brine with the increasing regulatory pressure [3].

Membrane distillation (MD) technique, driven by the vapor pressure difference across a hydrophobic medium [4], is widely recognized as a promising method for brine management as a result of its excellent effluent quality, relatively less energy consumption, and higher salt tolerance [5–7]. It has been confirmed that RO brine could be enriched by nearly 40 times in MD units, obtaining a rather considerable water recovery rate higher than 98% [8]. However, membrane fouling issue, especially membrane

* Corresponding author.

scaling, is generally confirmed as a crucial obstacle for the industrial-scale applications of MD units into the disposal of RO brine [9,10], highly attributing to the sedimentation of several sparingly soluble minerals like $CaSO_4$, $CaCO_3$, silicate, etc. Scaling induced a remarkable attenuation of membrane lifespan, even causing the occurrence of membrane wetting and then the dramatic penetration of brine across the MD membrane [11,12]. Comparatively, the precipitations of $CaSO_4$ and $CaCO_3$ are widely reported to be the two main scaling types in MD system [13].

The alkaline scaling like $CaCO_3$ was found to be partially mitigated through the optimization of operation conditions, for example lowering the feed temperature and acidifying feed to pH 4 [14]. However, the feed temperature of MD plants should be maintained at a certain level to ensure the considerable production of permeate solution. The mitigation of $CaCO_3$ scaling through the decrement of feed temperature might not be a feasible solution for MD system. Although the pH adjustment could significantly remove HCO_3^- from feed solutions, the huge usage of acid suggested that pH adjustment was not an economic strategy for the long-term MD treatment of RO brine [15]. Additionally, various membrane cleaning solutions have been also implemented for the elimination of scaling layer from MD membranes [16], while frequent membrane cleaning would gradually induce wetting phenomenon and salt leakage [17,18]. A widely applied industrial strategy for scaling control is the dose of trace amounts (<10 mg/L) of low-cost antiscalants [19].

Antiscalant is a common tool to control membrane crystallization through these next mechanisms: (1) postponing the nucleus formation of salt crystals; (2) decreasing sedimentation rate of crystals; (3) destroying crystal forms; and (4) altering CO_2 concentration [20,21]. Several commercial antiscalants including condensed polyphosphates, organophosphates, and polyelectrolytes, have been currently applied to some conventional desalination plants like RO. In view of the low cost and high anti-scaling efficiency, phosphorus antiscalants of phosphates and phosphonates were the major commercial antiscalants for scaling mitigation in RO system [22–24]. Hasson et al. [25] applied phosphates-type antiscalants (SHMP) into RO devices for the scale suppression of $CaCO_3$, and found that a tiny dosage (2.0 mg/L) of SHMP can effectively retard the RO flux drop that induced by $CaCO_3$ scaling. The phosphates-type antiscalants like SHMP exerted their anti-scaling performance mainly through the formation of soluble complex with salt ions or distortion of crystal lattice [26]. However, the usage of phosphates in RO system existed the risk of calcium phosphate scaling and biofouling as a result of their hydrolyzation [27], thus the phosphonates-type antiscalants gradually superseded phosphates in the real RO operation [28,29]. Several researches tested the scale inhibition efficiency of commercial organophosphonate antiscalants (LB-0100, Permatreat 191, Vitec 2000, etc.,) in RO plants, and the results indicated that organophosphonate antiscalants provided superior performance to phosphates due to their higher stability and superior dispersion of silt, clay, and metal oxides [22,30,31]. To restrict the phosphorus emissions, several phosphorus-free antiscalants (synthetic polymeric antiscalants) are presently researched for the scaling inhibition, and the polycarboxylic acid (PAA, polymethacrylic acid, polymaleic acid, etc.,) is reported to be the main type [29,32]. Shmulevsky et al. [33] applied polycarboxylic acid-based antiscalant for the mtigation of calcium sulfate scaling in RO system, and found that polycarboxylic acid-type antiscalant could effectively prolong the induction period through the crystal distortion effect. Except for the polycarboxylic-type, synthetic polymeric antiscalants with other functional groups (PAA/sulfonic acid/sulfonated styrene) also exhibited considerable performance for $CaCO_3$ inhibition in RO plants [34,35]. Furthermore, some environment-friendly antiscalants like PASP and PESA is presently springing up due to their biodegradable property [36,37]. In summary, phosphonates and polycarboxylic acid are two major types of antiscalants for scaling inhibition in real RO system in view of their low cost and efficient anti-scaling performance [38]. Similarly, the above-mentioned antiscalants have also been applied in MD system to explore their scale inhibition performance. Gryta [39] applied polyphosphate-based antiscalants for the regulation of $CaCO_3$ scaling in MD units, and the obtained results suggested that the issue of $CaCO_3$ crystals could be effectively resolved via the appropriate addition of this polyphosphate-based antiscalant. Cho et al. [40] compared the scaling control performance of 7 types of antiscalants during the MD purification of water generating from shale-gas drilling, and found that the crystal-inhibition efficiency of antiscalants was mainly ascribed to their specific chemical compositions and structures. The previous researches of scaling mitigation by antiscalants mostly focused on the comparison of scaling-inhibition efficiency among different types of antiscalants. Different from other membrane separation processes like RO, MD is a thermal-driven process (40°C–80°C), and the thermal condition of feed side might pose inevitable impacts on the anti-scaling efficiency of these antiscalants that widely used in normal temperature process. Additionally, the previous researches mainly evaluated the anti-scaling efficiency of phosphate-based antiscalants in MD desalination units. It is still unclear whether these antiscalants that are efficient in RO devices could still mitigate the membrane scaling and wetting in MD system. And the impacts of MD feed temperature on anti-scaling mechanisms and performance of antiscalants in MD system need to be further researched.

Accordingly, the mitigation of calcium carbonate precipitation by three different types of antiscalants was studied in this work, including 1-hydroxyethylidene-1,1-diphosphonic acid (HEDP), polyamino polyether methylene phosphonic acid (PAPEMP), and hydrolyzed polymaleic anhydride (HPMA). The combined effects of feed temperature, antiscalant type, and antiscalant concentration were comprehensively explored in this study. The anti-scaling performance of these three antiscalants was carefully compared from several aspects of feed quality, permeation quality, and permeate flux variation. To better understand how $CaCO_3$ scaling occurs during the MD treatment of RO brine as well as its mitigation mechanisms by antiscalants, a scanning electron microscope (SEM) coupled with an energy-dispersive X-ray spectroscopy (EDS) and X-ray

diffraction (XRD) analysis were conducted to exhibit the crystal structure and morphology of $CaCO_3$ scaling layer on the MD membrane surfaces, and map the element composition along the cross-section of fouled membranes. Additionally, the influence of MD feed temperature on $CaCO_3$ scaling mitigation by three different types of antiscalants was researched at different feed temperatures ranging from 40°C to 90°C. The anti-scaling performance at different antiscalant dosages of 5–100 mg/L was also investigated in this study. This work aimed to evaluate an efficient solution to mitigate $CaCO_3$ scaling for a sustainable application of MD system in the reuse disposal of RO brine.

2. Materials and methods

2.1. Membranes and feed water

The hydrophobic polytetrafluoroethylene (PTFE) membrane (Membrane Solutions, America) was applied for the MD operation in this study. According to the manufacturer, the porosity, pore size, thickness, and contact angle of PTFE membrane were 75%–80%, 0.22 μm, 190.0 ± 2.5 μm, and 130°C ± 2°C, respectively. A patch of PTFE membrane (12 cm × 7 cm) was embedded into a direct contact membrane distillation (DCMD) module. The PTFE membrane was soaked into deionized (DI) water for around 24 h before use.

A simulated RO brine was prepared with $NaHCO_3$ (10018960, Sinopharm), NaCl (73522260, Sinopharm), and $CaCl_2$ (10005860, Sinopharm) to investigate $CaCO_3$ scaling in DCMD system. The characteristics of the simulated RO brine are summarized in Table S1.

Three commercial antiscalants of HEDP, PAPEMP, and HPMA were chosen to study their scaling inhibition performance for $CaCO_3$ during MD disposal of RO brine. The characteristic properties of each antiscalant are shown in Table S2 and Fig. S1. The dosage gradient of antiscalants in MD plants was determined based on their practical applications in traditional thermal desalination devices, ranging from 5 to 100 mg/L.

2.2. DCMD operation

MD experiments were carried out for around 72 h with simulated RO brine in a self-manufactured DCMD device (Fig. 1). The DCMD plant was established with a feed tank, a thermostat water bath (HH-2, KEXI Instrument, China), a MD module, a permeate tank, a cryogenic thermostatic bath (XODC-0506, Deju Equipment Limited Company, China), an electronic balance (BS-3000+, Yousheng, China), a computer, and two peristaltic pumps (BT100-2J, Longer, England). The cross-flow velocity of solutions in these two sub-systems was both kept at around 10.5 mm/s with the control of two peristaltic pumps. The temperature of permeate side was continuously controlled at 15°C. The temperature of MD feed side was set as 60°C during the experimental research of antiscalant type and dosage. During the investigation of scaling mitigation of three antiscalants under different feed temperatures, four feed temperatures of 40°C, 60°C, 80°C, and 90°C were applied in this work. All the fouling experiments were repeated twice in this study to avoid the occasionality of experimental data.

Material of polymerized methylmethacrylate, namely perspex, was utilized for the manufacture of MD module, in which the two water channels for feed and permeate sides posed a space size of 50 mm width, 100 mm length, and

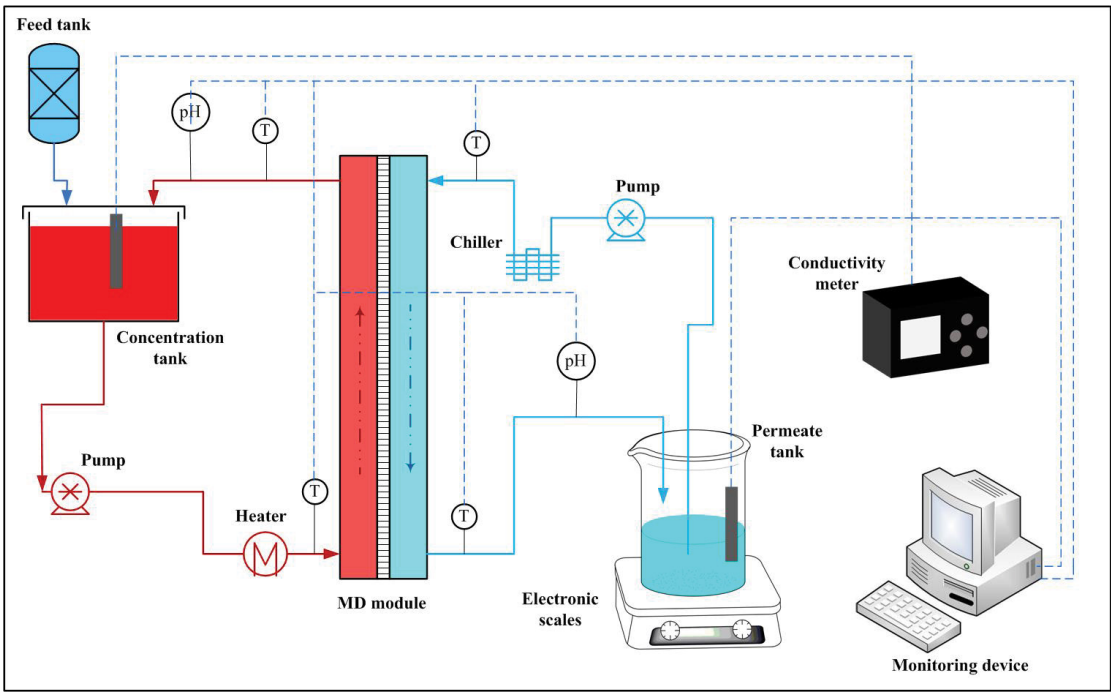

Fig. 1. Experimental setup of the direct contact membrane distillation plant.

2 mm height. A piece of PTFE membrane with an effective area of around 50 cm^2 was placed into the DCMD module. To enhance the water permeation in the MD module, two pieces of spacers with a thickness of around 1.0 mm were severally embedded inside the above-mentioned two flow channels. Distillate water in permeate side was continuously collected and then weighted via the electronic balance, and the weight data were recorded with a computer every 10 min. To track the variations of MD permeability, the index of normalized flux (NF) was calculated by the proportion of permeate flux (J) and initial flux (J_0).

2.3. Analytical methods

The solution samples were daily collected from the feed and permeate sides of MD unit to monitor changes in of pH and conductivity via a multi-parameter water quality analyzer (HQ30D, HACH, America) equipped with a pH electrode (PHC301, HACH, America) and a conductivity electrode (HQd, HACH, America). Additionally, the daily-sampled feed solutions were also applied for the measurements of dissociative metal ions (Ca^{2+} and Na^{+}) through an inductively coupled plasma-atomic emission spectrometry (ICP-AES, Thermo iCAP 6300, America). In each repeated experiment, the water quality measurements of each solution sample were conducted for at least three times, and the averages of measured results are presented in this study.

Concerning the membrane scaling characterization, several membrane coupons were cut from the fouled membrane samples to explore the deposition of salt crystals on the MD membrane surface via an X-ray diffractometer (XRD, D8 DISCOVER, Bruker, Germany) and a scanning electron microscope (SEM, S-4800, HITACHI, Japan) coupled with energy dispersive spectrometer (EDS, Octane Plus, Ametek, America). The XRD and SEM-EDS data from one repeated experiment are presented in this study. The detailed description about each test method is specifically listed in the Supplementary Information section III.

3. Results and discussions

3.1. Influence of antiscalant type on the $CaCO_3$ mitigation performance

3.1.1. MD performance

3.1.1.1. Permeate flux decline

Fig. 2 displays the impacts of antiscalant type on membrane flux over time, and the results revealed that a sharp flux decline from 1.0 (NF, 0 h) to 0.30 (NF, 72 h) was obtained for the MD system without antiscalants. At the end of MD operation (72 h), the final NF of MD membrane was obviously mitigated to around 0.67 (HEDP), 0.69 (PAPEMP), and 0.75 (HPMA) with the antiscalant dosage of 20 mg/L and the most outstanding anti-scaling performance was obtained for HPMA.

After 72 h operation of RO brine, the fouled PTFE membranes were removed from the MD module and then

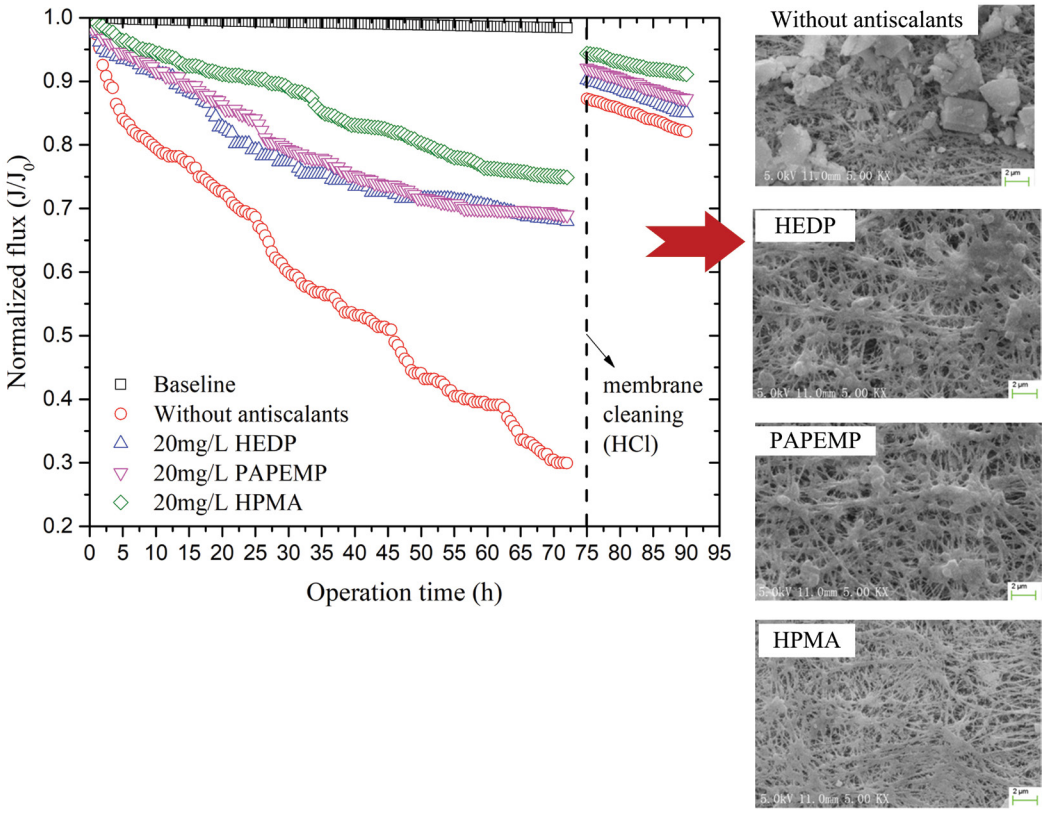

Fig. 2. Flux decline curves for MD operation of RO brine with or without antiscalants addition; and SEM images of fouled membrane surfaces that cleaned by 2 wt.% HCl solution. (Feed temperature: 60°C; distillate temperature: 15°C; antiscalant dosage: 20 mg/L).

washed with 2 wt.% HCl solutions for about 30 min. During the membrane cleaning process, several bubbles can be observed from the membrane surfaces, and the deposited precipitations gradually disappeared from the fouled membranes. After chemical cleaning, the NF of fouled membranes were recovered to 0.87 (without antiscalants), 0.90 (HEDP), 0.92 (PAPEMP), and 0.94 (HPMA), respectively (Fig. 2). Comparatively, the membrane flux recovery was more remarkable for these experimental groups with antiscalants usage, suggesting that the dosage of antiscalants induced a milder scaling layer that could be easily removed from the MD membrane surface. In comparison with HEDP and PAPEMP groups, the optimal scale inhibition performance was obtained for the HPMA group due to its higher NF after membrane cleaning.

3.1.1.2. Water quality variation

With the usage of different antiscalants, the variations of water qualities in feed and permeate sides are shown in Figs. 3 and 4 and Table S3. The pH and conductivity of initial feed solutions were 7.8 and 12.5 mS/cm, respectively. Without the presence of antiscalants, the conductivity of feed solutions finally changed to around 38.2 mS/cm after 72 h MD operation. Upon the application of antiscalants, the final conductivity of feed solutions partly increased, which was even close to 50 mS/cm. Moreover, the concentration of salt ions (Ca^{2+} and Na^{+}) in feed side also increased with operation time, as shown in Fig. 4. And the increment rate of Na^{+} was relatively higher than that of Ca^{2+}, highly owing to the gradual formation of $CaCO_3$ precipitations. Owing to the rise of Ca^{2+} concentration in MD feeds, the salts of calcium carbonate were supersaturated and then gradually crystallized from the feed solutions. After 72 h MD run, the MD feed solution without antiscalants exhibited a rather low concentration of Ca^{2+} (1.88 g/L), which was due to that Ca^{2+} and HCO_3^- largely formed $CaCO_3$ crystals on the MD membrane. With the presence of antiscalants, notable increment of Ca^{2+} concentration was obtained for feed solutions, with the highest value for the HPMA group (3.15 g/L, 72 h). This result further confirmed that HPMA exerted a better anti-scaling performance in MD system, highly mitigating the precipitation of $CaCO_3$ scales on the MD membranes.

Without the addition of antiscalants, the final conductivity of permeate solution gradually increased to 62.0 μS/cm (72 h), which was distinctly higher than other groups. Upon the dose of 20 mg/L antiscalants into MD feed, the final conductivity of permeate side was all lower than 15 μS/cm (72 h). The distinctly higher conductivity in permeate solutions suggested that the MD system without antiscalants might exist a membrane wetting phenomenon, resulting in the gradual deterioration of permeation quality.

3.1.2. Membrane scaling analysis

The mineral scales formed on the MD film under four experimental groups were detailedly researched via XRD analysis, as shown in Fig. 5. Three crystalline peaks at 18.2°, 22.8°, and 25.9° (Fig. S2) were detected on the XRD spectra of PTFE membranes in four experimental groups, representing the semicrystalline polymer of PTFE [41]. Except for the characteristic peaks of PTFE membrane material, other peaks at 29.3°, 33.2°, 38.8°, 42.8°, 45.8°, and 56.2° also existed on the XRD spectra of PTFE films, revealing the appearance of calcite, aragonite, and vaterite on the MD membranes. With the addition of antiscalants, the peaks for calcite precipitations were clearly reduced, and more peaks for vaterite crystals appeared on the XRD spectra. This phenomenon was extremely significant for HPMA group, confirming the outstanding $CaCO_3$ inhibition performance of HPMA. Therefore, it can be surmised that the presence of HEDP, PAPEMP, and HPMA in MD system could partly transform the crystal forms of $CaCO_3$, from stable calcite to loose aragonite and vaterite, leading to the formation of an unstable scaling layer that can be easily washed away from the membrane surface. The formation of $CaCO_3$ scaling was achieved through three steps: (1) precipitation of amorphous $CaCO_3$ from the supersaturated solutions; (2) transformation of amorphous $CaCO_3$ to metastable aragonite and vaterite; and (3) transformation of metastable aragonite and vaterite to the stable calcite [35]. The functional groups of antiscalants (carboxyl and phosphonyl groups) could be absorbed onto the active growth sites of the (104) face of calcite, blocking the growth of crystal nucleus by impeding the collision among crystal faces [42]. Additionally, those active growth sites were also the active dissolution points of vaterite, thus the dissolution of metastable vaterite was notably hindered by the antiscalants [42]. Based on the dissolution-recrystallization mechanism [43], the transformation of vaterite to calcite was realized through the dissolution of metastable vaterite and the nucleation growth of calcite. With the application of antiscalants, this kind of transformation was gradually restricted, leading to the stable existence of vaterite or aragonite in MD feed side. These three types of antiscalants exhibited different capacities of changing the crystal form of $CaCO_3$, highly attributing to the chelating ability of different functional groups as well as the matching property among antiscalants and crystal surfaces.

To further explore the effects of antiscalant type on $CaCO_3$ scaling in MD system, the morphology and element composition of fouled membranes were studied via SEM-EDS analysis. As shown in Fig. S3, the fibrous microporous structure can be seen from the surface of virgin PTFE membrane, and C and F were the two main elements. With 72 h-MD operation of simulated RO brine, the PTFE membrane surface was covered with a scaling layer, which was mainly constituted of $CaCO_3$ crystals with three different crystal forms (Fig. 6a1–d1). Without the usage of antiscalants, the calcite with regular hexahedron structure was the main crystal form for $CaCO_3$ scaling, posing smooth surface and sharp edge (red circle in Fig. 6a1). Upon the addition of antiscalants, the size of $CaCO_3$ crystals was partly reduced, and obvious variations were observed for the morphology of scaling layer. Concretely, the scaling layer became looser, and the $CaCO_3$ precipitations exhibited a rough surface with fractures. With the dose of 20 mg/L HEDP, the crystal form of deposited $CaCO_3$ changed to needlelike aragonite (blue circle in Fig. 6b1), with lower thermodynamic stability than calcite. With the addition of 20 mg/L PAPEMP, the deposited scales on the membranes

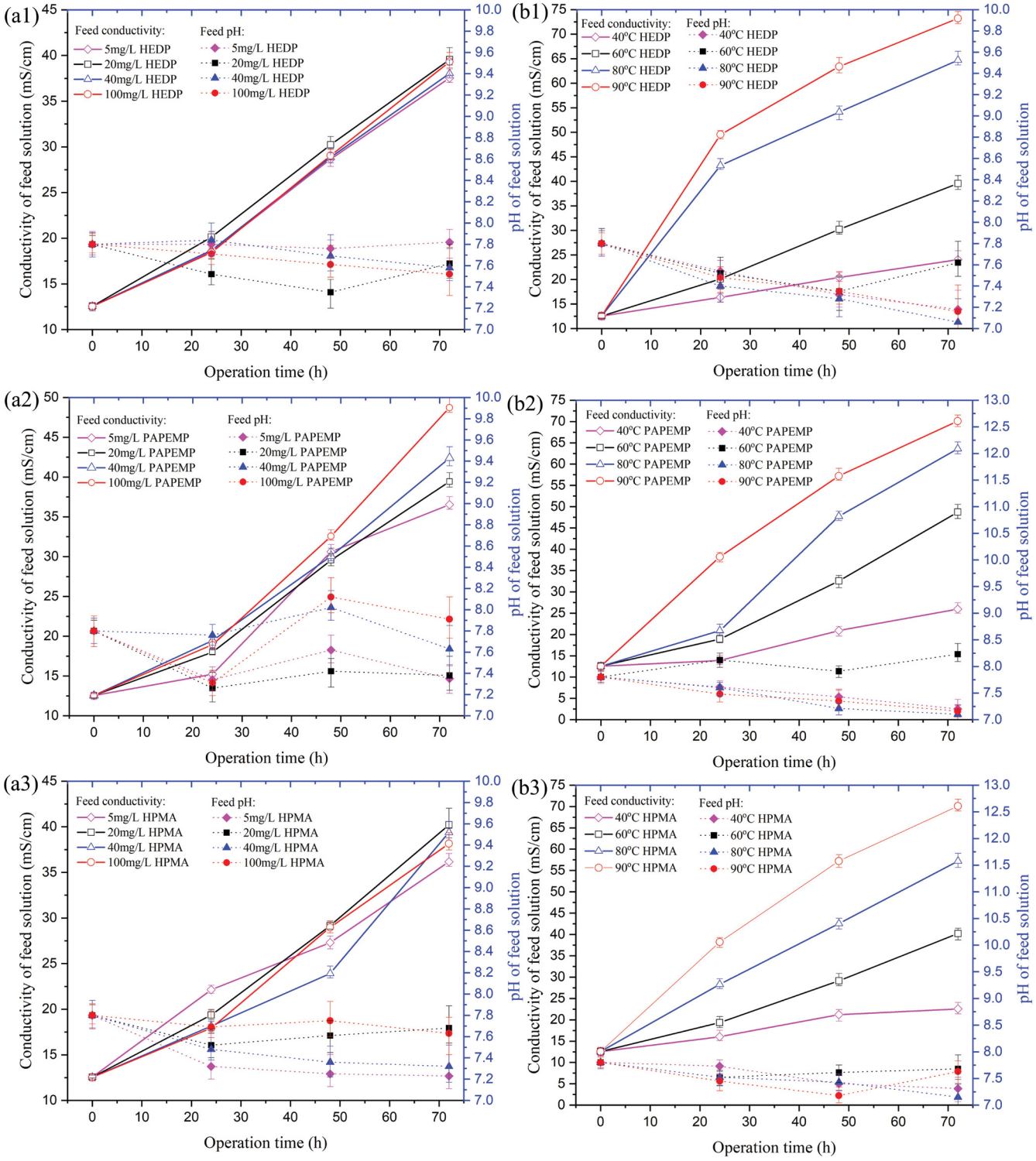

Fig. 3. Variations of feed water quality (conductivity and pH) under effects of feed temperature and antiscalant dosage. ((a1–a3) feed temperature: 60°C; distillate temperature: 15°C, (b1) antiscalant dosage: 20 mg/L, (b2) antiscalant dosage: 100 mg/L, and (b3) antiscalant dosage: 20 mg/L).

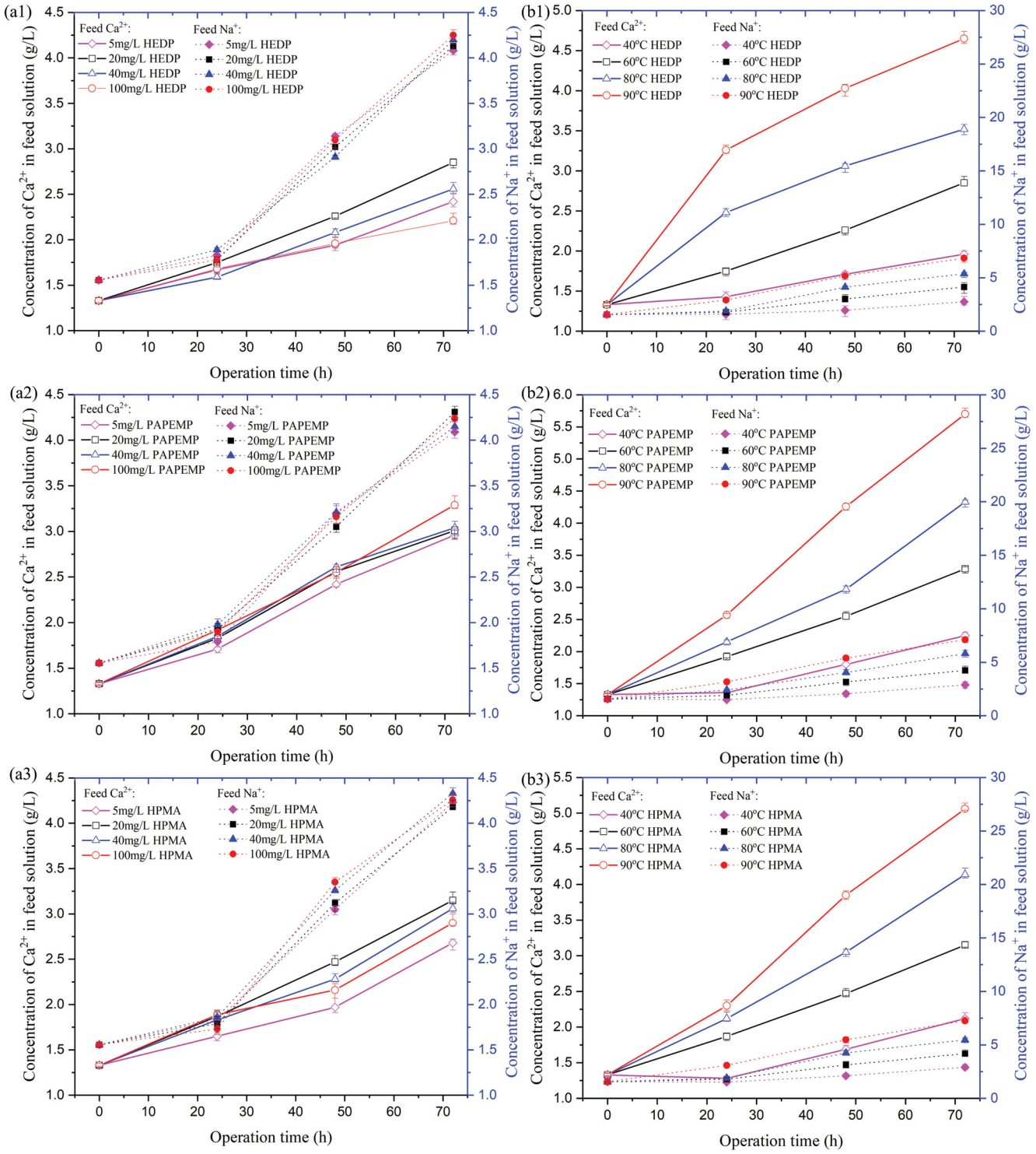

Fig. 4. Variations of feed water quality (Ca^{2+} and Na^{+} concentration) under effects of feed temperature and antiscalant dosage. ((a1–a3) feed temperature: 60°C; distillate temperature: 15°C, (b1) antiscalant dosage: 20 mg/L, (b2) antiscalant dosage: 100 mg/L, and (b3) antiscalant dosage: 20 mg/L).

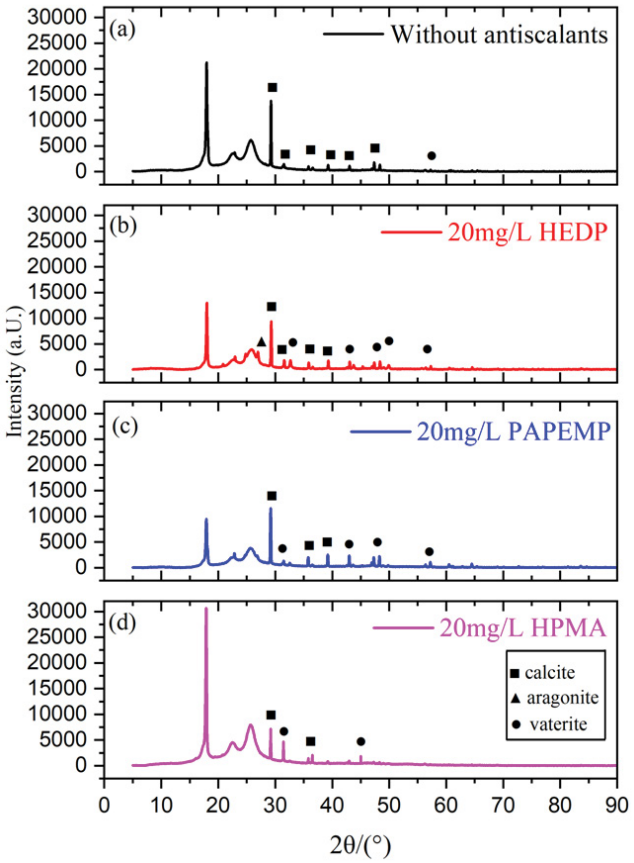

Fig. 5. XRD spectra of fouled PTFE membranes. (Feed temperature: 60°C; distillate temperature: 15°C; antiscalant dosage: 20 mg/L).

mostly consisted of spherical vaterite (green circle in Fig. 6c1), and its thermodynamic stability was relatively lower than calcite and aragonite. Comparatively, the most drastic variation of crystal morphology was obtained for HPMA group, and the deposited $CaCO_3$ crystals were nearly constituted of small vaterite with a smooth surface (1–2 μm, Fig. 6d1). The specific structure of virgin PTFE could still be remarkably observed from the membrane surface of HPMA group (black arrow in Fig. 6d1), further confirming the higher anti-scaling efficiency of HPMA. With the absence of antiscalants, the MD membrane exhibited a rather high intensity of Ca element (123 CPS/keV, Fig. 6a2) on the membrane surface. With the presence of antiscalant, the intensity of Ca element on the membrane surface was reduced to 104 CPS/keV (HEDP, Fig. 6b2), 88 CPS/keV (PAPEMP, Fig. 6c2), and 32 CPS/keV (HPMA, Fig. 6d2), respectively. Except for the Ca element, a trace of P element could also be detected from the fouled membrane surfaces, partly due to the slight existence of calcium phosphate scales on the MD film. As shown in Fig. 6d2, significant F element (101 CPS/keV) can be detected from the fouled membrane surface of HPMA group, manifesting that the MD film was slightly deposited by $CaCO_3$ crystals and the virgin PTFE structure can still be largely observed from the membrane surface.

Moreover, the SEM-EDS analysis of membrane cross-section was also applied, and the results are well displayed in Fig. 7. Basing on the element composition of C, F, and Ca along the membrane cross-section, the active layer of PTFE (B → C), the PET supporting layer (C → D), and the scaling layer (A → B) can be clearly distinguished from cross-section of fouled PTFE membrane (Fig. S3). It can be seen from Fig. 7a–d that the addition of antiscalants in MD system could remarkably decrease the thickness of scaling layer, with the lowest layer thickness for the HPMA group. Without the usage of antiscalants, the Ca element can be largely detected from the membrane surface and pores, exhibiting a severe $CaCO_3$ scaling on the PTFE surfaces and pores (Fig. 7e). This result revealed that the issue of membrane wetting already emerged in MD system after 72 h operation of RO brine, resulting in a sharp deterioration of distillation quality. With the dose of HEDP and PAPEMP, the intensity of Ca element was clearly reduced along the membrane cross-section, revealing their considerable anti-scaling effects for $CaCO_3$ in MD system. However, the Ca element can still be detected from the PTFE pores in HEDP and PAPEMP groups, suggesting the mediocre mitigation performance for membrane wetting in MD system. Differently, the Ca element was mainly found on the membrane surface of HPMA group, and nearly no $CaCO_3$ penetrated into the PTFE pores. This phenomenon suggested that the anti-scaling performance of HPMA was better than HEDP and PAPEMP, and the membrane wetting issue could be well solved with the application of HPMA.

After 72 h-MD operation of RO brine, the fouled PTFE membranes were further conducted with chemical cleaning (2 wt.% HCl solution) for 30 min, and the SEM images of cleaned membrane surfaces are shown in Fig. 2. With the HCl cleaning, the deposited scaling layer was clearly removed from the fouled PTFE membrane surfaces, and the virgin PTFE structure appeared on the MD surface. Comparatively, several residual scales still existed on the PTFE surface of blank group (without antiscalant), while nearly no $CaCO_3$ precipitation was retained on the PTFE surface of HPMA group. The usage of antiscalants in MD system would destroy the crystal lattice of $CaCO_3$, which changed from stable calcite to aragonite and vaterite with lower thermodynamic stability. Hence, a loose and thin inorganic layer finally formed on the MD membrane, which could be easily washed away from the membrane surface.

3.1.3. Comparison of anti-scaling efficiency of three types of antiscalants

The anti-scaling efficiency of antiscalants (dosage of 20 mg/L) was calculated basing on the measured Ca^{2+} concentrations and concentration ratios of feed solutions, which were around 49%, 54%, and 61% for HEDP, PAPEMP, and HPMA, respectively.

In terms of molecular structure, HEDP and PAPEMP were both methylene phosphonic acid compounds, which could increase the solubility of calcium salts in feed solutions by forming chelates with Ca^{2+}. HEDP molecule posed two negatively charged phosphate groups, which could be easily combined with Ca^{2+} through strong electrostatic

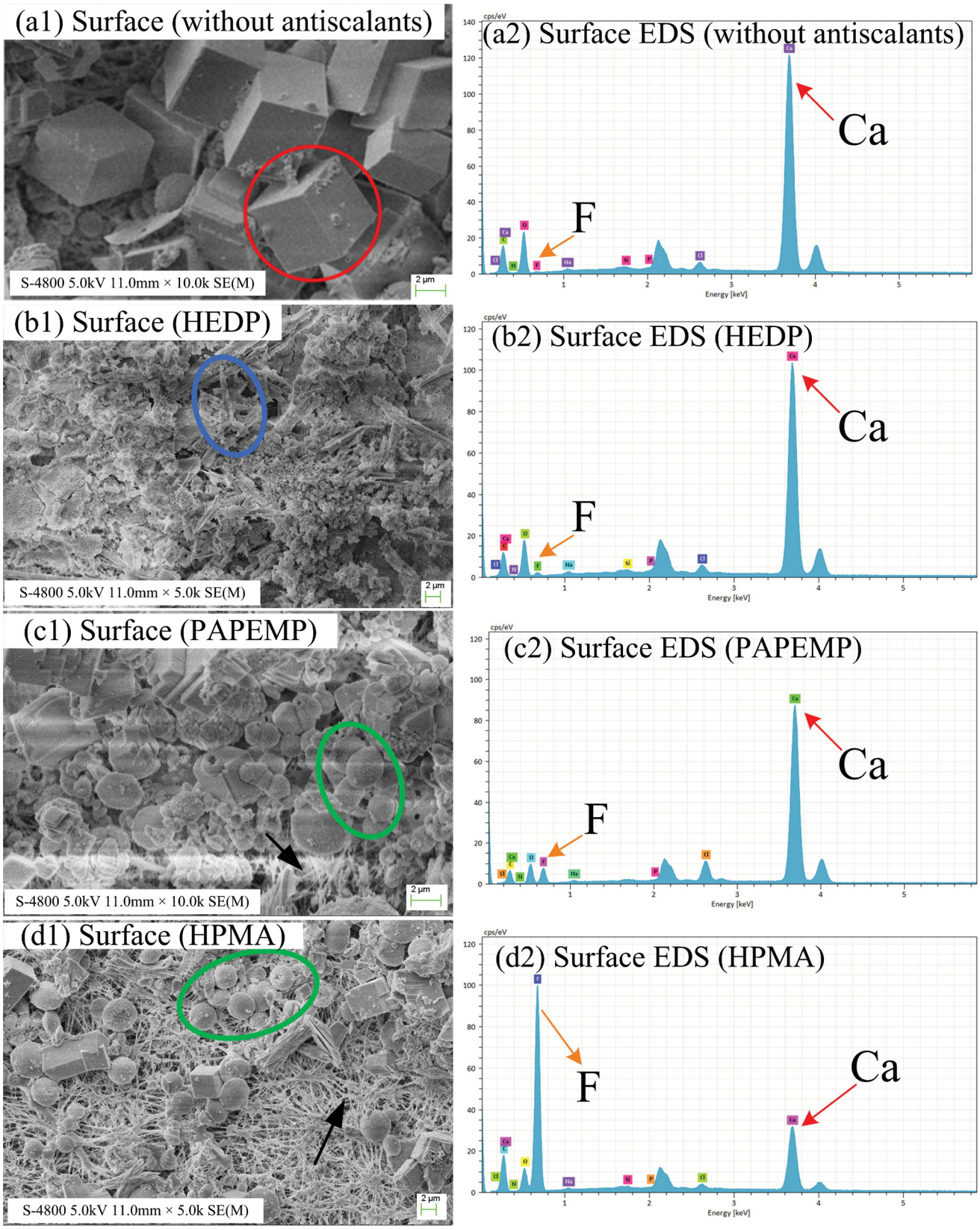

Fig. 6. SEM membrane surface analysis of fouled membranes (a1–d1) and EDS analysis of fouled membrane surfaces (a2–d2). (Feed temperature: 60°C; distillate temperature: 15°C; antiscalant dosage: 20 mg/L).

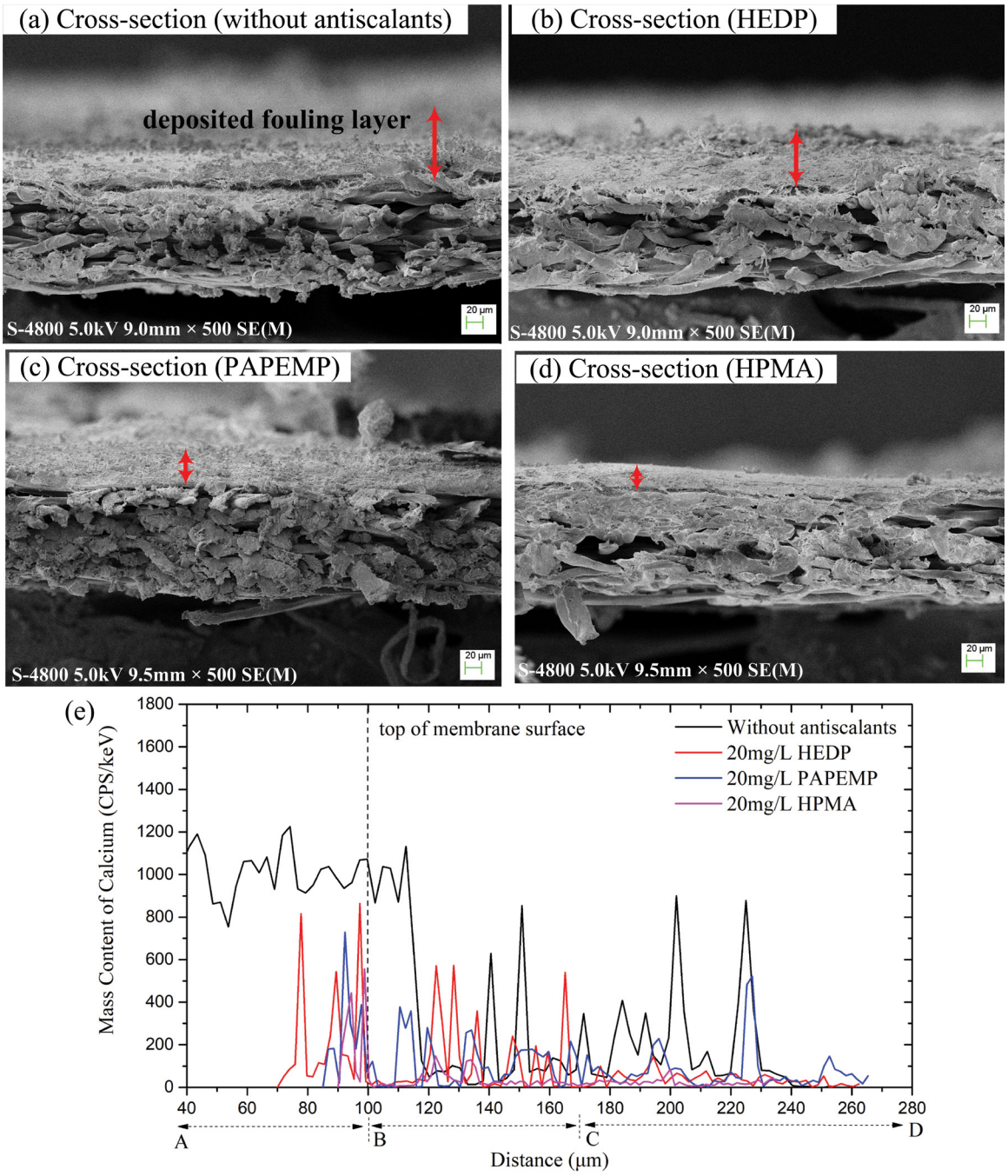

Fig. 7. Cross-section SEM images of fouled membranes (a–d) and mass content of Ca element as a function of membrane depth (e). (Feed temperature: 60°C; distillate temperature: 15°C; antiscalant dosage: 20 mg/L).

interactions to form two five-membered ring chelates, so as to inhibit the growth of $CaCO_3$ crystals on the MD membranes. Similarly, the PAPEMP molecule could form five five-membered ring chelates with Ca^{2+}, inducing a higher anti-scaling efficiency than HEDP. Moreover, PAPEMP molecule also possessed a unique ether group, inevitably enhancing the chelating solubilization among PAPEMP and Ca^{2+}, thus synergistically increased its anti-scaling efficiency for $CaCO_3$ in MD system.

HPMA was a kind of polycarboxylate-type antiscalant, which could significantly improve the solubility of $CaCO_3$ in feed solutions through the chelation among Ca^{2+} and active carboxyl groups of HPMA molecules. Additionally, HPMA could interact with the active sites of crystal nucleus, and then remarkably changed the morphology and crystalline phase of calcium carbonate precipitations [44], leading to the formation of a rather mild scaling layer on the MD film surface. Owing to the specific interactions

among antiscalants and calcium ions, HPMA exhibited an outstanding $CaCO_3$ mitigation in MD system, which was followed by PAPEMP and HEDP.

3.2. Effect of antiscalant dosage on the $CaCO_3$ mitigation performance

The permeate flux decline trends of MD system under different dosage of antiscalants are exhibited in Fig. 8, suggesting that antiscalant dosage posed distinct effects on the anti-scaling efficiency. In terms of HEDP, the most obvious $CaCO_3$ mitigation was obtained for the dosage of 20 mg/L, and the NF was finally changed to about 0.68 (72 h, Fig. 8a). With the HEDP dosage of 5, 40 and 100 mg/L, the final NF of MD membrane was decreased to 0.63 (5 mg/L), 0.56 (40 mg/L) and 0.54 (100 mg/L), respectively. The result suggested that the higher dosage of HEDP in MD system would unexpectedly deteriorate the anti-scaling efficiency, and a moderate increment of HEDP dosage to around 20 mg/L might be a considerable choice. Comparatively, the dosage demonstrated an extremely remarkable impact on the $CaCO_3$ mitigation performance of PAPEMP, as shown in Fig. 8b. The higher dosage strengthened the anti-scaling efficiency of PAPEMP in MD system, and the final NF of MD membrane was continuously increased from 0.57 to 0.82 as the dosage increased from 5 to 100 mg/L. Comparatively, PAPEMP exhibited an unique scaling mitigation behavior, that is a better anti-scaling performance induced by the higher antiscalant dosage. For HPMA, the optimum $CaCO_3$ mitigation performance was observed for the dosage of 20 mg/L, and the final NF of PTFE membrane was nearly 0.75 (Fig. 8c). A too high or too low dosage of HPMA in MD system both caused a certain decay of anti-scaling efficiency for $CaCO_3$ crystals.

Fig. 3a displays that feed conductivity was clearly increased with MD operation time, while the pH of feeds exhibited a certain reduction during the MD run. In the thermal circumstance, the formation of $CaCO_3$ partly resulted in the generation of H^+ in feed solutions, thus led to the slight decrement of pH in feeds. Regardless of the antiscalant dosage, the conductivity of feeds was continuously increased with the operation time, highly attributing the concentration process of salts in feed side. The most significant increment of feed conductivity occurred at the antiscalant dosage where optimum anti-scaling efficiency was obtained, which was 20, 100, and 20 mg/L for HEDP, PAPEMP, and HPMA, respectively. The membrane flux was rather high at the optimum antiscalant dosage, resulting in a higher concentration rate of feed solutions and then a faster increment of feed conductivity. Hence, the concentrations of Ca^{2+} and Na^+ in feed solutions also exhibited increments with the operation time regardless of antiscalant dosage (Fig. 8c). As shown in Table S3, the pH of distillation was kept at a relatively stable level of 6.53–7.23, while a clear fluctuation of conductivity can be seen for MD permeate side. Comparatively, the most remarkable fluctuation of permeation conductivity was observed for HEDP and PAPEMP groups, which sharply increased with the MD run. In terms of HEDP, the permeation conductivity finally increased to 39.22, 13.58, 38.26, and 52.39 μS/cm at the dosage of 5, 20, 40, and 100 mg/L, suggesting the partial membrane wetting still existed in the HEDP group. Differently, the permeation conductivity of HPMA group was kept at a relatively low level of 5.78–12.43 μS/cm, revealing that nearly no membrane wetting phenomenon occurred with the application of HPMA in MD system.

The morphologies of scaling layers formed under the different antiscalant dosages are displayed in Fig. 8. Regardless of the HEDP dosage, the MD membrane surface was covered with a scaling layer of calcite, aragonite, and vaterite, and the size of $CaCO_3$ crystals was decreased in comparison with the blank group (without antiscalants). In terms of the HEDP dosage of 5, 40, and 100 mg/L, the deposited layer was prevailingly consisted of calcite and vaterite, inducing a more severe scaling behavior than the dosage of 20 mg/L. With the dosage of 20 mg/L HEDP, the PTFE membrane surface was mostly deposited by aragonite and several loose slags with lattice distortion, finally leading to a milder scaling phenomenon. The EDS analysis of fouled membranes revealed that the dosage of 20 mg/L HEDP could partly reduce the intensity of Ca element on the membrane surface in comparison with other HEDP dosages (Fig. S4). In terms of PAPEMP, the deposition of $CaCO_3$ crystals on the MD membrane was clearly decreased with the increment of PAPEMP dosage. As shown in Fig. 8, the deposition of calcite and vaterite can still be observed from the PTFE surfaces with the PAPEMP dosage of 5 and 20 mg/L, and the deposited calcite largely exhibited a rough surface with fractures. However, with the further increment of PAPEMP dosage, the calcite and vaterite obviously disappeared from the membrane surfaces, and the PTFE membrane was mostly occupied by these loose and porous slags, thus notably mitigated the permeate flux decline trend. The EDS analysis of fouled membrane surfaces revealed that the intensity of Ca element in scaling layer decreased from 94 to 52 CPS/keV as the dosage increased from 5 to 100 mg/L (Fig. S4), further confirming that increasing dosage would clearly improve the $CaCO_3$ mitigation performance of PAPEMP. As regarding the HPMA, the mildest scaling layer was seen as 20 mg/L HPMA was added into the MD system, and the virgin PTFE structure can also be largely found from the fouled PTFE surface (Ca intensity of 100 CPS/keV). In HPMA group, the precipitations deposited on the membranes were mostly pony-sized vaterite as well as several aberrant calcite with notable fractures. The scaling layers formed at the dosage of 5 and 100 mg/L were both denser than other fouled membranes (40 and 20 mg/L HPMA groups). The intensity of Ca on the membrane surfaces was 80 CPS/keV (5 mg/L), 31 CPS/keV (20 mg/L), 58 CPS/keV (40 mg/L) and 65 CPS/keV (100 mg/L) in HPMA group, respectively.

Generally, the antiscalant dosage demonstrated different impacts on the $CaCO_3$ mitigation performance of HEDP, PAPEMP, and HPMA. The usage of HEDP and HPMA in MD system both existed an optimum dosage of around 20 mg/L. Differently, the anti-scaling performance of PAPEMP in MD system was notably enhanced with the increment of dosage. With an overall consideration of MD performance and economic cost, the usage of HPMA in MD system for $CaCO_3$ mitigation might be a better strategy, which could achieve a considerable anti-scaling performance at the dosage of 20 mg/L that similar to PAPEMP at a higher dosage of 100 mg/L.

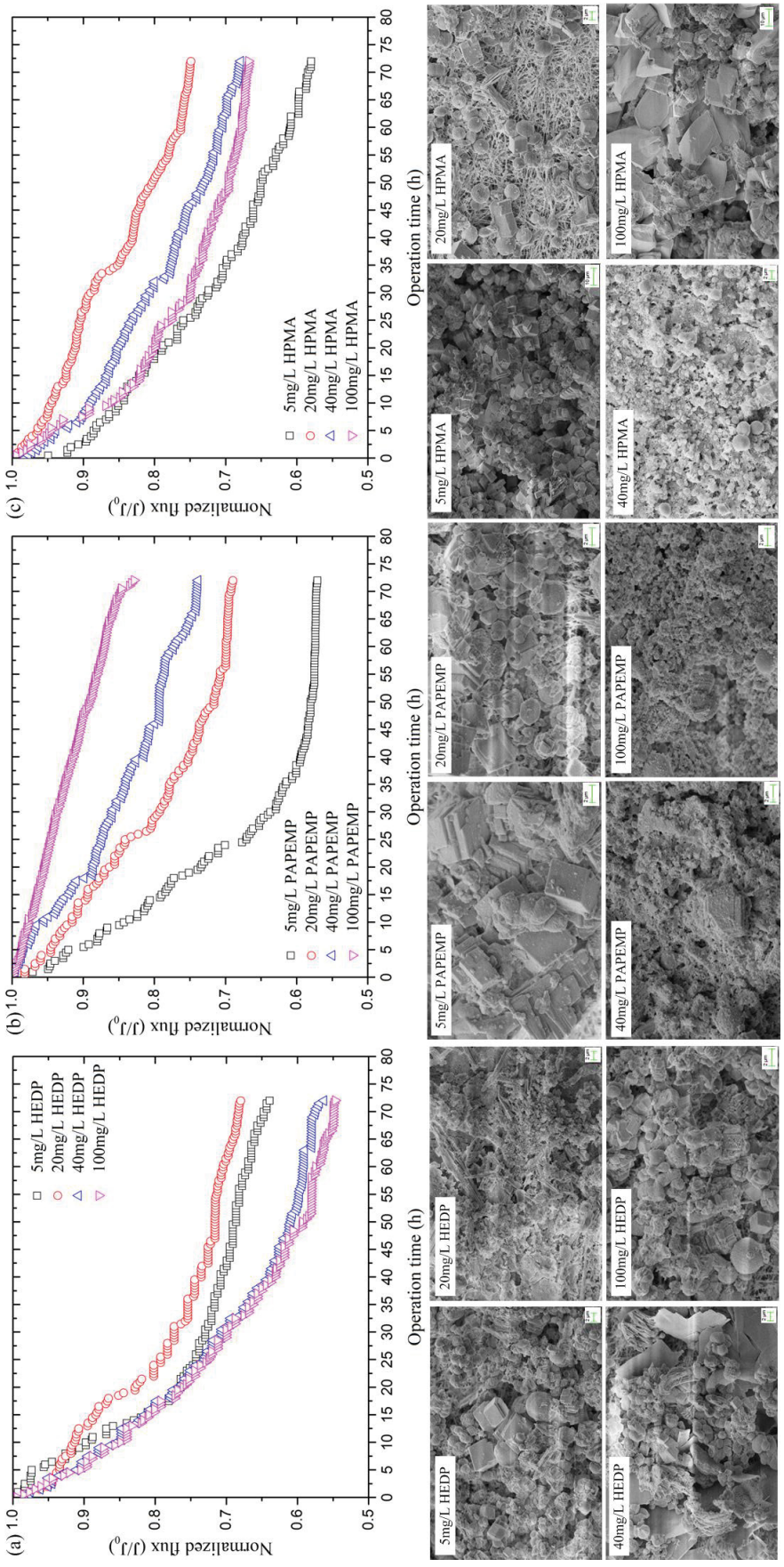

Fig. 8. Effects of dosage on performance of antiscalants in $CaCO_3$ scaling mitigation during DCMD process of RO brine: (a) HEDP, (b) PAPEMP, and (c) HPMA. (Feed temperature: 60°C; distillate temperature: 15°C).

3.3. Influence of feed temperature on $CaCO_3$ mitigation of antiscalants

3.3.1. Influence of feed temperature on anti-scaling performance of HEDP

Under the optimum dosage of 20 mg/L, the impacts of feed temperature on HEDP performance were researched in MD system, with four temperature gradients of 40°C, 60°C, 80°C, and 90°C. As shown in Fig. 9a, a relatively milder flux decline was obtained for 40°C and 60°C, which was finally changed to 0.77 (40°C) and 0.68 (60°C) at the end of MD run (72 h). Comparatively, a rather sharp and severe flux drop was seen for the MD run at 80°C and 90°C, which significantly decreased to around 0.39 (80°C) and 0.22 (90°C) after 72 h-MD operation. This result revealed that a moderate feed temperature would contribute to the anti-scaling performance of HEDP. Without the addition of antiscalants, the final NF of PTFE membrane was 0.61, 0.51, 0.31, and 0.16 under the MD feed temperature of 40°C, 60°C, 80°C, and 90°C, respectively. The dose of HEDP in MD system posed remarkable impacts on the membrane flux variation under the moderate feed temperature of 40°C and 60°C, and the NF of PTFE membrane was clearly improved by more than 15% with the presence of HEDP. However, the addition of HEDP in MD system exhibited a slight effect on the fouling mitigation under the higher feed temperature of 80°C and 90°C, suggesting that the increment of feed temperature might worsen the anti-scaling efficiency of HEDP in MD system. Although the water production efficiency of MD system could be largely improved by the increasing feed temperature, an aggravated flux decline trend would appeared in MD system. Firstly, the solubility of calcium carbonate reduced with the increasing feed temperature, thus more $CaCO_3$ would be precipitated from feed solutions under the higher feed temperature and then promoted the $CaCO_3$ scaling on the MD membrane. Additionally, the hydrolysis rate of HEDP would be enhanced by the increasing feed temperature, thus resulted in the attenuation of anti-scaling efficiency of HEDP and even induced risk of calcium phosphate scaling [45]. Moreover, the concentration rate of MD feed solution would be increased with the higher feed temperature, leading to the remarkable rise of Ca^{2+} concentration (Fig. 4b1) for the formation of insoluble organic phosphonate-calcium complexes in MD system and therefore an aggravated anti-scaling performance of HEDP.

The feed conductivity was continuously increased with MD operation, and a more notable increment was obtained for higher feed temperatures of 80°C and 90°C (Fig. 3b1). Under the higher feed temperature, a higher permeate flux was obtained for PTFE membrane and then induced a higher concentration rate of foulants in MD feeds, causing the clear rise of feed conductivity. Under the moderate feed temperature of 40°C and 60°C, the permeation conductivity was always maintained at a low level of 5.39–13.58 μS/cm during the whole MD run. With the rise of feed temperature (80°C and 90°C), the conductivity of permeate side existed a burst to a range of 45.23–65.20 μS/cm during the later MD run (Table S4), revealing that a slight wetting phenomenon appeared in MD units.

For the MD operation under higher feed temperature (80°C and 90°C), the obvious appearance of calcite was detected from the MD membrane surface, while the scale layer developed under the moderate feed temperature (40°C and 60°C) was mostly aragonite and aberrant slags (Fig. 9). Basing on the Ca^{2+} concentration, the $CaCO_3$ mitigation efficiency of HEDP was approximately 46%, 49%, 35%, and 34% under the feed temperature of 40°C, 60°C, 80°C, and 90°C, respectively. This result further confirmed that the moderate feed temperature was beneficial for the anti-scaling performance of HEDP in MD system.

3.3.2. Influence of feed temperature on anti-scaling performance of PAPEMP

With the antiscalant dosage of 100 mg/L, the influence of MD feed temperature on the $CaCO_3$ mitigation performance of PAPEMP was studied, and the membrane decline trends are well presented in Fig. 9b. The NF of PTFE membrane was finally decreased to about 0.86, 0.82, 0.62, and 0.51 under the feed temperature of 40°C, 60°C, 80°C, and 90°C, respectively. The anti-scaling efficiency of PAPEMP for $CaCO_3$ crystals was continuously kept at a considerable range of 65%–69% in MD system, with the highest value obtained for high feed temperature of 90°C, revealing that PAPEMP could still pose a well anti-scaling performance under the extremely high temperature. Regardless of the feed temperature, the permeate conductivity of PAPEMP group was always lower than that of HEDP group, with a range of 5.78–22.51 μS/cm (Table S4). Although the MD feed temperature remarkably increased the Ca^{2+} concentration in feed solutions (Fig. 4b2), a considerable anti-scaling efficiency was still obtained for PAPEMP, likely due to that PAPEMP posed a high tolerance to calcium salts through the outstanding chelation among Ca^{2+} and PAPEMP molecules. Regardless of feed temperature, the PTFE membrane surface was mainly occupied by large amounts of aberrant slags and several vaterite (Fig. 9) with the presence of 100 mg/L PAPEMP in MD system, resulting in a relatively mitigated scaling behavior. Totally, the MD feed temperature exhibited milder impacts on the anti-scaling efficiency of PAPEMP, and the PAPEMP still posed a considerable mitigation performance for $CaCO_3$ in the extremely thermal condition of MD system.

3.3.3. Influence of feed temperature on anti-scaling performance of HPMA

Under the optimum dosage of 20 mg/L, the anti-scaling performance of HPMA under different feed temperatures was explored in MD system, and the variations of permeate flux are clearly presented in Fig. 9c. The final NF of PTFE membrane was continuously maintained at a high level of 0.57–0.87 under the feed temperature of 40°C–80°C, while that significantly dropped by 66% as the feed temperature further raised to 90°C. The anti-scaling efficiency of HPMA in MD system was higher than 60% as the feed temperature was lower than 80°C. However, the anti-scaling efficiency of HPMA was notably decreased to approximately 47% when the MD feed temperature rose to 90°C. This result suggested that the feed temperature lower than 80°C posed a rather mild impact on the anti-scaling performance of HPMA, while the anti-scaling efficiency of HPMA would be obviously deteriorated as the MD feed

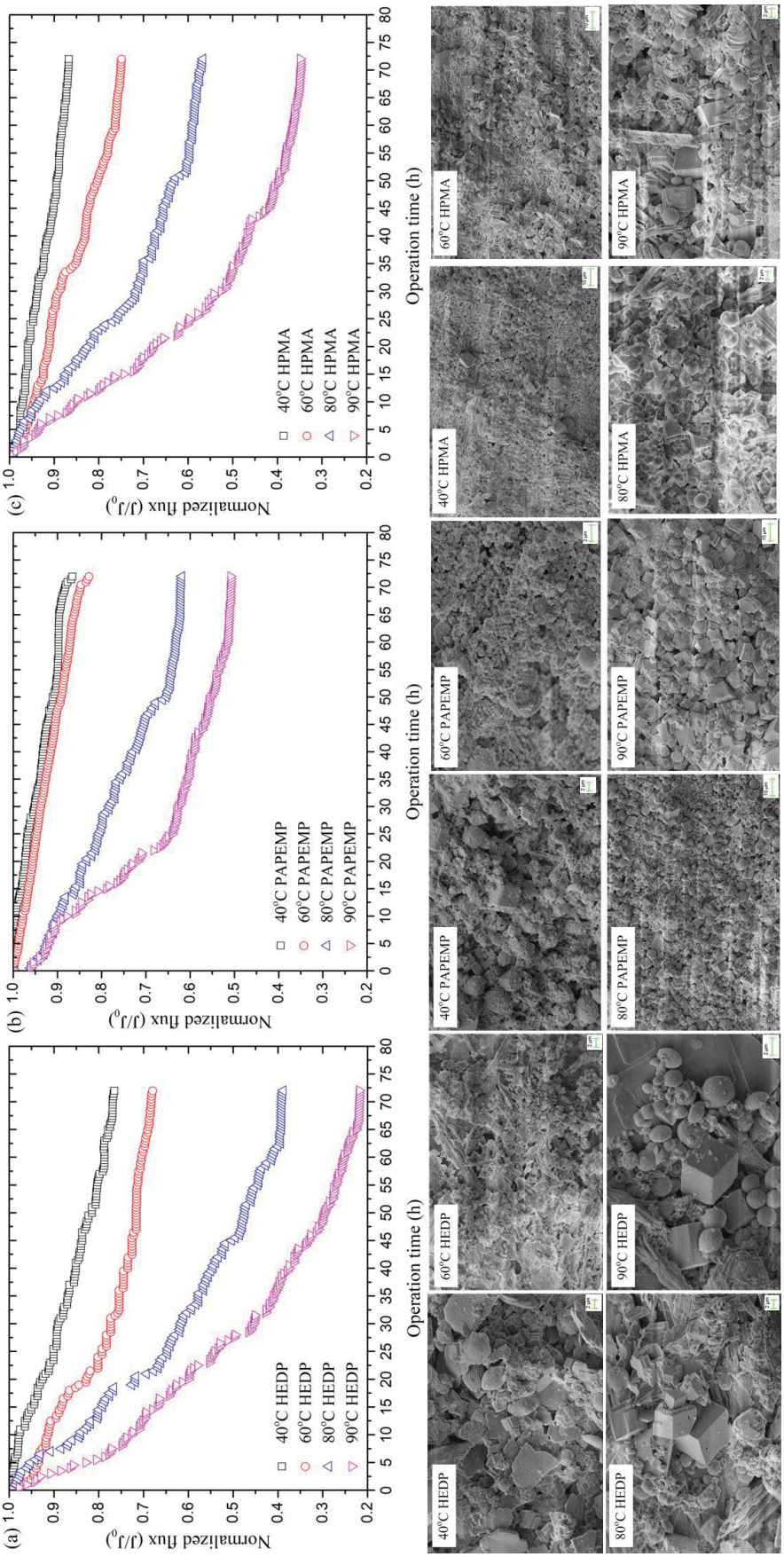

Fig. 9. Effects of feed temperature on performance of antiscalants in $CaCO_3$ scaling mitigation during DCMD process of RO brine: (a) HEDP, (b) PAPEMP, and (c) HPMA. (Distillate temperature: 15°C; dosage of HEDP, PAPEMP and HPMA was 20, 100 and 20 mg/L, respectively).

temperature further increased to 90°C. The clear decrement of anti-scaling efficiency might be associated with the reducing solubility of calcium carbonate and the high concentration rate of feed solutions under the extremely high feed temperature. Regardless of the feed temperature, the permeation conductivity was always kept in a stable and low range of 3.61–17.53 μS/cm (Table S4), suggesting that nearly no membrane wetting occurred in MD system with the usage of HPMA. As shown in Fig. 9, the PTFE membrane was mildly deposited by several vaterite and distorted calcite with fractures when feed temperature was lower than 80°C. And the virgin PTFE structure can still be remarkably observed from the fouled PTFE surfaces. As the feed temperature further raised to 90°C, large-sized calcite with a regular shape clearly appeared on the PTFE membrane surface, further confirming that the extremely high feed temperature (>80°C) might pose a non-negligible impact on the $CaCO_3$ mitigation performance of HPMA in MD system.

3.4. Scale inhibition mechanisms of three types of antiscalants in DCMD system

HEDP posed two phosphonyl groups, forming chelate complexes with Ca^{2+}, thus partly increased the solubility of calcium salts. Additionally, HEDP molecules could bind with the active sites of $CaCO_3$ nucleus, destroying the lattice structure of $CaCO_3$ crystals, hence the deposited scaling layer on the MD membrane became relatively loose. With the moderate dosage, HEDP exhibited a considerable anti-scaling performance in MD system, while the $CaCO_3$ mitigation efficiency of HEDP was clearly decreased with the further increment of dosage, namely threshold effect [46]. Under the higher HEDP dosage, the redundant HEDP molecules would form insoluble floccules (organic phosphonate-calcium complex) in MD feed side, causing the deterioration of HEDP performance in MD plants. The feed temperature of MD system demonstrated remarkable impacts on the anti-scaling efficiency of HEDP, and a good anti-scaling performance of HEDP was obtained under the moderate feed temperature of 40°C and 60°C. The high feed temperature would partly cause the hydrolysis of HEDP molecules, inducing a risk of calcium phosphate scaling.

PAPEMP posed a prominent tolerance to calcium salts, which could interact with the active sites of $CaCO_3$ nucleus to prevent the further growth of $CaCO_3$ crystals. Moreover, PAPEMP molecules could be embedded in the lattice of $CaCO_3$ crystals, increasing the surface tension of nucleus and changing the crystal form, thus formed an unstable scaling layer. Although HEDP and PAPEMP molecules posed similar functional groups of phosphonyl groups, a clear distinction of $CaCO_3$ mitigation performance was seen between HEDP and PAPEMP, which might be associated with the length of carbon chain and other functional groups of antiscalant molecule. PAPEMP molecules could form more five-membered ring chelates with Ca^{2+}, inducing a better anti-scaling efficiency than HEDP. Moreover, PAPEMP molecules also possessed a unique ether group, forming more complex and stable chelates with Ca^{2+}, synergistically increasing its anti-scaling efficiency for $CaCO_3$ in MD system. The $CaCO_3$ mitigation performance of PAPEMP in MD system was obviously improved by the increasing dosage, which was mildly affected by MD feed temperature. The increasing antiscalant dosage remarkably enhanced the anti-scaling efficiency of PAPEMP during the MD operation of RO brine, while a high dosage of chemical agents would inevitably increase the operational cost of MD system.

HPMA molecule contained active carboxyl groups, forming soluble complexes with Ca^{2+}, thus exhibited a good mitigation performance for $CaCO_3$ scaling. Additionally, HPMA molecules could be adsorbed onto the active sites of $CaCO_3$ crystal nucleus, inhibiting the growth of crystals and then increasing the solubility of calcium salts. Without the presence of antiscalants, the deposited $CaCO_3$ crystals were mostly hexahedral calcite with a regular structure. Upon the addition of HPMA, the structure of deposited precipitations was notably changed, and the fouling layer was largely consisted of vaterite with small size and rough surfaces. Generally, the presence of HPMA in MD system would inhibit the growth of calcite, which was obviously transformed to vaterite with lower thermodynamic stability. According to the dissolution-recrystallization mechanism, the transformation from vaterite to calcite was obtained through the dissolution of vaterite nucleus and then the nucleation of calcite. However, the active sites of $CaCO_3$ crystals occupied by HPMA were the dissolution points of vaterite, highly blocking the transformation from vaterite to calcite. Considering the lower thermodynamic stability of vaterite, a rather mild and loose scaling layer mostly consisted of vaterite and aberrant slags ultimately developed on the MD membrane with the addition of HPMA in MD system. To achieve a well anti-scaling performance for $CaCO_3$, MD operation of RO brine with the presence of 20 mg/L HPMA under the feed temperature lower than 80°C might be a feasible choice.

4. Conclusions

In this work, the impacts of three types of antiscalants were explored on $CaCO_3$ mitigation during the MD treatment of RO brine, and the effects of feed temperature and antiscalant dosage were also researched. Key findings from our work can be summarized as follows:

- The addition of HEDP, PAPEMP, and HPMA in feed solutions all posed considerable anti-scaling performance for $CaCO_3$ scaling and partly mitigated membrane wetting. PAPEMP and HPMA exceeded HEDP in postponing the flux decline trends of MD membranes.
- These three types of antiscalants couldn't absolutely restrain the occurrence of $CaCO_3$ scaling in MD system but efficiently transformed the structure of deposited $CaCO_3$ crystals from stable calcite to labile forms of vaterite and aragonite.
- The antiscalant dosage exhibited a notable impact on the $CaCO_3$ mitigation performance of three types of antiscalants. For HEDP and HPMA, the $CaCO_3$ scaling can be well mitigated at the dosage of 5–20 mg/L. Differently, the anti-scaling efficiency of PAPEMP could be obviously improved by increasing dosage.
- The anti-scaling performance of HEDP in $CaCO_3$ scaling inhibition was significantly temperature-dependent, and the increasing feed temperature deteriorated the

scaling mitigation performance. The high feed temperature would cause the hydrolysis of HEDP molecules, inducing a risk of calcium phosphate scaling for MD membranes. Comparatively, PAPEMP and HPMA posed greater tolerance to feed temperature, which still exhibited a considerable anti-scaling performance under a high feed temperature of 80°C.

- With a comprehensive consideration, HPMA outperformed PAPEMP and HEDP in mitigating $CaCO_3$ scaling and membrane wetting during MD process of RO brine. HPMA with moderate dosage (<20 mg/L) could still perform outstanding $CaCO_3$ inhibition under the high feed temperature (80°C), and nearly no membrane wetting phenomenon occurred in MD plants. With the presence of HPMA, a rather loose and thin scaling layer mostly constituting of vaterite and aberrant slags was mildly developed on the MD membranes, which could be significantly removed by HCl cleaning with a remarkable recovery of membrane flux.

Acknowledgements

This work was basically financially supported by National Natural Science Foundation of China (grant number: 52100107) and Natural Science Foundation of Jiangsu Province (grant number: BK20210829).

References

[1] J.-H. Shim, J.-Y. Jeong, J.-Y. Park, SWRO brine reuse by diaphragm-type chlor-alkali electrolysis to produce alkali-activated slag, Desalination, 413 (2017) 10–18.
[2] N. Ghaffour, T.M. Missimer, G.L. Amy, Combined desalination, water reuse, and aquifer storage and recovery to meet water supply demands in the GCC/MENA region, Desal. Water Treat., 51 (2013) 38–43.
[3] A. Panagopoulos, K.-J. Haralambous, M. Loizidou, Desalination brine disposal methods and treatment technologies - a review, Sci. Total Environ., 693 (2019) 133545, doi: 10.1016/j.scitotenv.2019.07.351.
[4] H.-C. Kim, J. Shin, S. Won, J.-Y. Lee, S.K. Maeng, K.G. Song, Membrane distillation combined with an anaerobic moving bed biofilm reactor for treating municipal wastewater, Water Res., 71 (2015) 97–106.
[5] M.R. Qtaishat, F. Banat, Desalination by solar powered membrane distillation systems, Desalination, 308 (2013) 186–197.
[6] E. Curcio, X. Ji, G. Di Profio, E. Fontananova, E. Drioli, Membrane distillation operated at high seawater concentration factors: role of the membrane on $CaCO_3$ scaling in presence of humic acid, J. Membr. Sci., 346 (2010) 263–269.
[7] A. Razmjou, E. Arifin, G. Dong, J. Mansouri, V. Chen, Superhydrophobic modification of TiO_2 nanocomposite PVDF membranes for applications in membrane distillation, J. Membr. Sci., 415 (2012) 850–863.
[8] Q. Dan, J. Wang, L. Wang, D. Hou, Z. Luan, B. Wang, Integration of accelerated precipitation softening with membrane distillation for high-recovery desalination of primary reverse osmosis concentrate, Sep. Purif. Technol., 67 (2009) 21–25.
[9] E. Curcio, X. Ji, G. Di Profio, E. Fontananova, E. Drioli, Membrane distillation operated at high seawater concentration factors: role of the membrane on $CaCO_3$ scaling in presence of humic acid, J. Membr. Sci., 346 (2010) 263–269.
[10] Z. Yan, H. Yang, F. Qu, H. Zhang, H. Rong, H. Yu, H. Liang, A. Ding, G. Li, B. Van der Bruggen, Application of membrane distillation to anaerobic digestion effluent treatment: identifying culprits of membrane fouling and scaling, Sci. Total Environ., 688 (2019) 880–889.
[11] L.D. Nghiem, T. Cath, A scaling mitigation approach during direct contact membrane distillation, Sep. Purif. Technol., 80 (2011) 315–322.
[12] H. Maab, A. Al Saadi, L. Francis, S. Livazovic, N. Ghafour, G.L. Amy, S.P. Nunes, Polyazole hollow fiber membranes for direct contact membrane distillation, Ind. Eng. Chem. Res., 52 (2013) 10425–10429.
[13] A. Anvari, K.M. Kekre, A. Ronen, Scaling mitigation in radio-frequency induction heated membrane distillation, J. Membr. Sci., 600 (2020) 117859, doi: 10.1016/j.memsci.2020.117859.
[14] M. Gryta, Alkaline scaling in the membrane distillation process, Desalination, 228 (2008) 128–134.
[15] M. Gryta, Polyphosphates used for membrane scaling inhibition during water desalination by membrane distillation, Desalination, 285 (2012) 170–176.
[16] L.D. Tijing, Y.C. Woo, J.-S. Choi, S. Lee, S.-H. Kim, H.K. Shon, Fouling and its control in membrane distillation—a review, J. Membr. Sci., 475 (2015) 215–244.
[17] F. Qu, Z. Yan, H. Yu, G. Fan, J. He, Effect of residual commercial antiscalants on gypsum scaling and membrane wetting during direct contact membrane distillation, Desalination, 486 (2020) 114493, doi: 10.1016/j.desal.2020.114493.
[18] H.C. Duong, S. Gray, M. Duke, T.Y. Cath, L.D. Nghiem, Scaling control during membrane distillation of coal seam gas reverse osmosis brine, J. Membr. Sci., 493 (2015) 673–682.
[19] P. Zhang, P. Knötig, S. Gray, M. Duke, Scale reduction and cleaning techniques during direct contact membrane distillation of seawater reverse osmosis brine, Desalination, 374 (2015) 20–30.
[20] D.M. Warsinger, J. Swaminathan, E. Guillen-Burrieza, H.A. Arafat, Scaling and fouling in membrane distillation for desalination applications: a review, Desalination, 356 (2015) 294–313.
[21] H. Elcik, L. Fortunato, A. Alpatova, S. Soukane, J. Orfi, E. Ali, H. AlAnsary, T. Leiknes, N. Ghaffour, Multi-effect distillation brine treatment by membrane distillation: effect of antiscalant and antifoaming agents on membrane performance and scaling control, Desalination, 493 (2020) 114653, doi: 10.1016/j.desal.2020.114653.
[22] A. Rahardianto, W.-Y. Shih, R.-W. Lee, Y. Cohen, Diagnostic characterization of gypsum scale formation and control in RO membrane desalination of brackish water, J. Membr. Sci., 279 (2006) 655–668.
[23] R. Semiat, I. Sutzkover, D. Hasson, Characterization of the effectiveness of silica anti-scalants, Desalination, 159 (2003) 11–19.
[24] W.-Y. Shih, A. Rahardianto, R.-W. Lee, Y. Cohen, Morphometric characterization of calcium sulfate dihydrate (gypsum) scale on reverse osmosis membranes, J. Membr. Sci., 252 (2005) 253–263.
[25] D. Hasson, R. Semiat, D. Bramson, M. Busch, B. Limoni-Relis, Suppression of $CaCO_3$ scale deposition by anti-scalants, Desalination, 118 (1998) 285–296.
[26] F. Rashchi, J. Finch, Polyphosphates: a review their chemistry and application with particular reference to mineral processing, Miner. Eng., 13 (2000) 1019–1035.
[27] B. Andrews, B. Davé, P. López-Serrano, S.-P. Tsai, R. Frank, M. Wilf, E. Koutsakos, Effective scale control for seawater RO operating with high feed water pH and temperature, Desalination, 220 (2008) 295–304.
[28] Y.M. Al-Roomi, K.F. Hussain, Application and evaluation of novel acrylic based $CaSO_4$ inhibitors for pipes, Desalination, 355 (2015) 33–44.
[29] J. Li, Y. Zhou, Q. Yao, T. Wang, A. Zhang, Y. Chen, W. Wu, W. Sun, Preparation and evaluation of a polyether-based polycarboxylate as a kind of inhibitor for water systems, Ind. Eng. Chem. Res., 56 (2017) 2624–2633.
[30] P. Bonné, J. Hofman, J. Van Der Hoek, Scaling control of RO membranes and direct treatment of surface water, Desalination, 132 (2000) 109–119.
[31] Q. Yang, Y. Liu, Y. Li, Control of protein (BSA) fouling in RO system by antiscalants, J. Membr. Sci., 364 (2010) 372–379.

[32] A.A. Al-Hamzah, C.M. Fellows, A comparative study of novel scale inhibitors with commercial scale inhibitors used in seawater desalination, Desalination, 359 (2015) 22–25.
[33] M. Shmulevsky, X. Li, H. Shemer, D. Hasson, R. Semiat, Analysis of the onset of calcium sulfate scaling on RO membranes, J. Membr. Sci., 524 (2017) 299–304.
[34] M. Dietzsch, M. Barz, T. Schüler, S. Klassen, M. Schreiber, M. Susewind, N. Loges, M. Lang, N. Hellmann, M. Fritz, K. Fischer, P. Theato, A. Kühnle, M. Schmidt, R. Zentel, W. Tremel, PAA-PAMPS copolymers as an efficient tool to control $CaCO_3$ scale formation, Langmuir, 29 (2013) 3080–3088.
[35] C. Tzotzi, T. Pahiadaki, S. Yiantsios, A. Karabelas, N. Andritsos, A study of $CaCO_3$ scale formation and inhibition in RO and NF membrane processes, J. Membr. Sci., 296 (2007) 171–184.
[36] B.K. Pramanik, Y. Gao, L. Fan, F.A. Roddick, Z. Liu, Antiscaling effect of polyaspartic acid and its derivative for RO membranes used for saline wastewater and brackish water desalination, Desalination, 404 (2017) 224–229.
[37] W. Yu, D. Song, A. Li, H. Yang, Control of gypsum-dominated scaling in reverse osmosis system using carboxymethyl cellulose, J. Membr. Sci., 577 (2019) 20–30.
[38] W. Yu, D. Song, W. Chen, H. Yang, Antiscalants in RO membrane scaling control, Water Res., 183 (2020) 115985, doi: 10.1016/j.watres.2020.115985.
[39] M. Gryta, Polyphosphates used for membrane scaling inhibition during water desalination by membrane distillation, Desalination, 285 (2012) 170–176.
[40] H. Cho, Y. Choi, S. Lee, J. Sohn, J. Koo, Membrane distillation of high salinity wastewater from shale gas extraction: effect of antiscalants, Desal. Water Treat., 57 (2016) 26718–26729.
[41] J. Watanabe, M. Akashi, Effect of an alternating current for crystallization of $CaCO_3$ on a porous membrane, Acta Biomater., 5 (2009) 1306–1310.
[42] K. Burns, Y.-T. Wu, C.S. Grant, Mechanisms of calcite dissolution using environmentally benign polyaspartic acid: a rotating disk study, Langmuir, 19 (2003) 5669–5679.
[43] A. Sarkar, S. Mahapatra, Mechanism of unusual polymorph transformations in calcium carbonate: dissolution-recrystallization vs. additive-mediated nucleation, J. Chem. Sci., 124 (2012) 1399–1404.
[44] Z. Shen, J. Li, K. Xu, L. Ding, H. Ren, The effect of synthesized hydrolyzed polymaleic anhydride (HPMA) on the crystal of calcium carbonate, Desalination, 284 (2012) 238–244.
[45] K. Karakulski, M. Gryta, A.W. Morawski, Membrane processes used for separation of effluents from wire productions, Chemical Pap. Slovak Acad. Sci., 63 (2009) 205–211.
[46] X. Li, B. Gao, Q. Yue, D. Ma, H. Rong, P. Zhao, P. Teng, Effect of six kinds of scale inhibitors on calcium carbonate precipitation in high salinity wastewater at high temperatures, J. Environ. Sci., 29 (2015) 124–130.

Supplementary information

S1. Section I

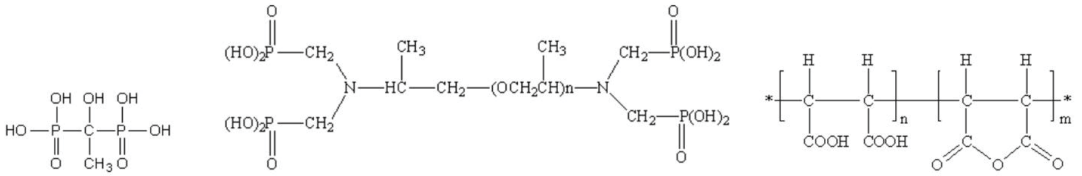

Fig. S1. Structural formula of each antiscalant.

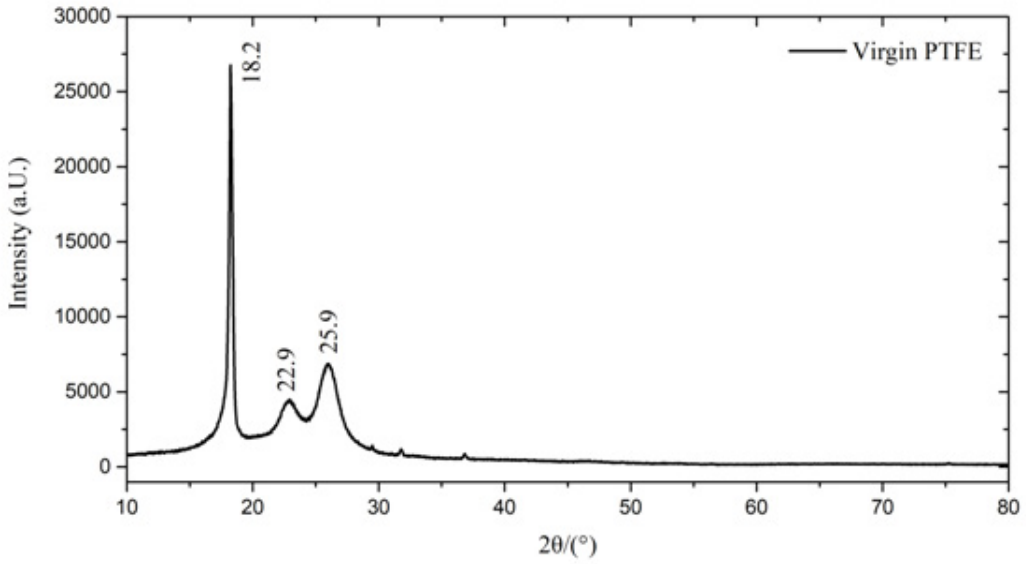

Fig. S2. XRD spectrum of virgin PTFE membrane.

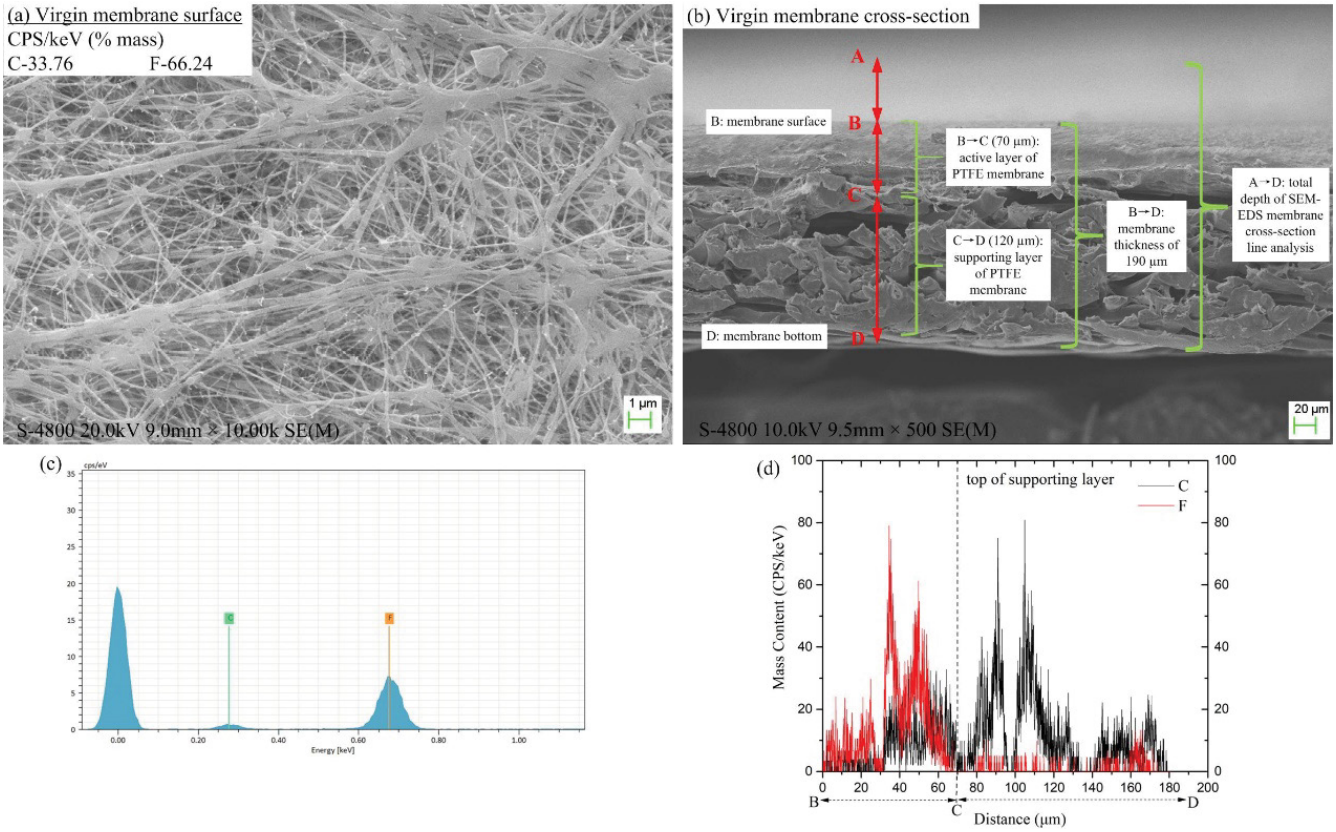

Fig. S3. The membrane surface (a) and cross-section (b) SEM images of virgin PTFE membrane; EDS membrane surface analysis (c) and cross-section line analysis (d) of virgin PTFE membrane.

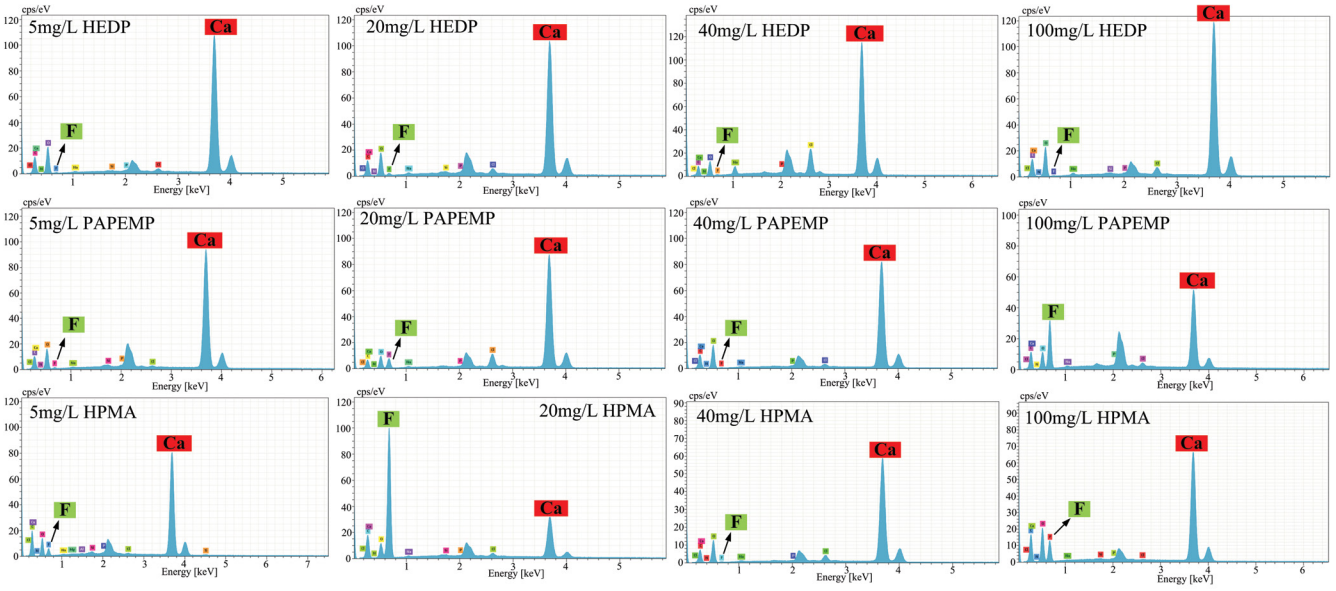

Fig. S4. EDS analysis of fouled membrane surfaces under the different dosage of three types antiscalants (Temperature difference: 60°C/15°C).

S2. Section II

Table S1
Characteristic properties of the simulated RO brine (water recovery of RO: 80%). The preparation of RO brine mainly concerned its $CaCO_3$ scaling tendency in membrane distillation units

Parameter, mM	Value
Ca^{2+}	33.1
Na^{+}	67.7
HCO_3^{-}	16.2
Cl^{-}	117.6
pH	7.8
TDS, mg/L	8,028
Conductivity, mS/cm	12.55

Table S2
Characteristic properties of each commercial antiscalant

Antiscalant type	Molecular formula	Manufacturer	Characteristic parameters of each antiscalant			
			Content of active component (%)	pH (in 1% aqueous solution)	Density (20°C, g/cm^3)	Optimum dosage suggested by manufacturer (mg/L)
HEDP	$C_2H_8O_7P_2$	KaiRui Water	≥50.0	≤2.0	1.34~1.40	1~50
PAPEMP	$C_{15}H_{40}O_{15}N_2P_4$	Treatment	≥40.0	≤2.0	1.15~1.25	5~100
HPMA	$(C_4H_4O_4)_n$	Technology Co., Ltd.	≥48.0	2.0~3.0	1.22~1.25	1~15

Table S3
Water quality of permeate solutions under different dosage of antiscalants

Dosage	Operation time (h)	Water quality parameters					
		pH			Conductivity (μS/cm)		
Type of antiscalants		HEDP	PAPEMP	HPMA	HEDP	PAPEMP	HPMA
5 mg/L	24	6.92 ± 0.23	7.07 ± 0.25	7.23 ± 0.25	7.26 ± 0.23	8.48 ± 0.22	7.68 ± 0.24
	48	6.68 ± 0.20	6.61 ± 0.22	6.91 ± 0.25	24.20 ± 0.33	21.46 ± 0.30	8.88 ± 0.22
	72	6.72 ± 0.20	6.53 ± 0.18	6.85 ± 0.22	39.22 ± 0.35	32.24 ± 0.28	12.43 ± 0.26
20 mg/L	24	6.96 ± 0.16	6.87 ± 0.23	6.96 ± 0.21	6.42 ± 0.18	5.32 ± 0.18	5.78 ± 0.17
	48	6.85 ± 0.20	6.85 ± 0.23	7.02 ± 0.27	7.35 ± 0.22	5.98 ± 0.17	6.86 ± 0.22
	72	6.96 ± 0.22	6.96 ± 0.20	6.95 ± 0.22	13.58 ± 0.25	12.65 ± 0.28	8.98 ± 0.25
40 mg/L	24	6.83 ± 0.22	7.02 ± 0.20	7.01 ± 0.22	9.54 ± 0.22	7.49 ± 0.22	6.86 ± 0.20
	48	6.76 ± 0.22	6.95 ± 0.22	6.96 ± 0.18	18.71 ± 0.25	9.75 ± 0.22	8.23 ± 0.18
	72	6.81 ± 0.25	6.92 ± 0.22	6.91 ± 0.18	38.26 ± 0.32	10.57 ± 0.24	9.81 ± 0.20
100 mg/L	24	6.89 ± 0.17	7.06 ± 0.23	7.12 ± 0.24	10.73 ± 0.20	8.03 ± 0.20	7.87 ± 0.25
	48	6.79 ± 0.21	7.02 ± 0.22	7.03 ± 0.22	21.28 ± 0.28	15.70 ± 0.20	9.32 ± 0.25
	72	6.78 ± 0.22	6.95 ± 0.20	6.88 ± 0.22	52.39 ± 0.35	25.30 ± 0.24	10.09 ± 0.30

Table S4
Water quality of permeate solutions under different feed temperatures

Feed temperature	Operation time (h)	Water quality parameters					
		pH			Conductivity (μS/cm)		
Type of antiscalants		HEDP	PAPEMP	HPMA	HEDP	PAPEMP	HPMA
40°C	24	7.11 ± 0.22	7.41 ± 0.25	7.22 ± 0.24	6.13 ± 0.22	6.35 ± 0.25	4.79 ± 0.16
	48	6.70 ± 0.20	7.12 ± 0.22	7.45 ± 0.24	6.52 ± 0.24	7.01 ± 0.25	5.84 ± 0.16
	72	6.45 ± 0.16	7.30 ± 0.22	7.18 ± 0.20	5.39 ± 0.22	5.78 ± 0.20	3.61 ± 0.18
60°C	24	6.96 ± 0.23	7.06 ± 0.23	6.96 ± 0.20	6.42 ± 0.20	8.03 ± 0.28	5.78 ± 0.22
	48	6.85 ± 0.18	7.02 ± 0.23	7.02 ± 0.20	7.35 ± 0.26	9.32 ± 0.28	6.86 ± 0.22
	72	6.96 ± 0.20	6.95 ± 0.17	6.95 ± 0.22	13.58 ± 0.28	10.09 ± 0.30	8.98 ± 0.20
80°C	24	7.02 ± 0.21	7.02 ± 0.20	6.92 ± 0.22	11.35 ± 0.25	8.18 ± 0.22	10.25 ± 0.24
	48	7.12 ± 0.24	7.12 ± 0.26	6.86 ± 0.16	41.50 ± 0.37	10.67 ± 0.22	7.86 ± 0.20
	72	6.96 ± 0.20	6.96 ± 0.20	7.13 ± 0.21	45.23 ± 0.40	15.36 ± 0.30	12.95 ± 0.22
90°C	24	6.93 ± 0.22	6.93 ± 0.20	6.85 ± 0.22	13.58 ± 0.22	11.27 ± 0.32	13.76 ± 0.25
	48	6.52 ± 0.14	6.52 ± 0.17	7.02 ± 0.22	60.48 ± 0.44	18.35 ± 0.30	17.53 ± 0.30
	72	6.86 ± 0.20	6.86 ± 0.20	6.76 ± 0.17	65.20 ± 0.44	22.51 ± 0.35	16.51 ± 0.32

S3. Section III

The specific description of analytical methods for foulants characterization in feed solution and membrane scaling characterization.

S4. Section IV

The specific description of analytical methods for foulants characterization in feed solution and membrane scaling characterization.

S4.1. Inductively coupled plasma-atomic emission spectrometry measurement

The concentrations of metals (Ca, Na) in feed solutions were measured using inductively coupled plasma-atomic emission spectrometry (ICP-AES; Thermo iCAP 6300, America). Prior to ICP-AES measurement, each sample was diluted with deionized water, and then filtered through an Acrodisc PES Syringe Filter (0.45 μm, Pall Corporation).

S4.2. Scanning electron microscopy-energy-dispersive X-ray spectroscopy measurement

A scanning electron microscopy (SEM; HITACHI S-4800) coupled with energy-dispersive X-ray spectroscopy (EDS; Octane Plus, Ametek) was applied for the investigation of surface morphology and elemental composition of virgin and fouled membranes. Furthermore, the cross-section line analysis was also conducted for the fouled membranes with an aim to verify the blockage of contaminants in membrane pores. The parameters were listed as below: accelerating voltage (10 kV), beam current (0.4×10^{-10} Å) and working distance (8–10 mm). The fouled membrane samples were dried for 12 h in a constant temperature oven (50°C) for the SEM-EDS analysis of membrane surface. In terms of the membrane cross-section SEM-EDS analysis, the fouled membrane samples were pretreated with liquid nitrogen brittle fracture, following by drying for 12 h at 50°C for the cross-section SEM-EDS measurement.

S4.3. X-ray diffraction measurement

The mineral composition of precipitates that deposited on the fouled membrane distillation membrane surfaces was determined via the X-ray diffraction (XRD) analysis. In this study, the XRD measurement was performed with a Philips X'Pert PRO Diffractometer using CuKα radiation with a graphite monochromator, within the 2θ angle range of 10°–80°. The counting time, wavelength and power conditions were set as 1.0 s, 1.506 Å and 20 kV/30 mA, respectively.